УДК 520.88

# THE ROZHEN IMAGE PROCESSING PACKAGE AND SOME OF ITS APPLICATIONS

*Tsvetan B. Georgiev*

DEPARTMENT OF ASTRONOMY AND NATIONAL ASTRONOMICAL OBSERVATORY OF THE BULGARIAN ACADEMY OF SCIENCES

A FORTRAN IV program package using a PDP 11—34 minicomputer system is described. Its purpose is to extract the information from a single extended image and to present it in graphical appearance. A set of preparatory procedures secures analysis of the image and its background, calibration, smoothing by convolute and median filtering, etc. A few conclusive procedures output photometrical profiles, isophote maps, morphological functions, photometrical diagrams, residual images, etc. A set of applications on various images shows the possibilities of the package as well as the main results obtained by it till now.

Остаточное изображение получается как разница между необработанным изображением и сглаженным изображением. Анализ остаточного изображения дает ценную информацию о плохо выраженных вариациях локальной яркости исследуемого объекта. Этот метод испытывается для горячих точек солнечных пятен, выбросов кометы Галея, спиральной структуры галактик М 51, М 31, М 81 и моста между галактиками М 81 и М 82.

## 1. Introduction

The aim of the Rozhen Image Processing Package (RIPP) is to aid the quantitative investigation of the isolated images of galaxies, nebulas, planets, solar spots, etc. For the present, the RIPP does not ensure some special techniques as the large field photometry, the crowed field stellar photometry and the restoration of the images. So, the RIPP is powerful to solve numerous problems, and it was already used successfully in practice.

The RIPP is created in 1984—86 in the Rozhen observatory and corresponds to the stimplest basic ideas given in the issues [1—7] as well as in the surveys [8—10].

Three short communications about the RIPP were made earlier [11—13]. The purposes of this paper are to present the package wholly, to inform about some special approaches and to show various expedient applications.

## 2. General information

The principal view of the RIPP is given in Scheme 1. The system includes the source of digital images, a sequence of different procedures and a set of output materials. The interaction between the procedures and the disk memory, as well as the current message production is shown by dashed lines.

The usual source of digital images is a Joyce Loebl microdensitometer, but any source (e. g. a CCD) is admissible. The process goes away on a 256 Kb PDP 11—34 minicomputer system in multi-user mode, where only 64 Kb memory is usable by one user's task. Each image is a file stored on a 27 Mb hard disk. The current information as well as the final results go out on an alpha-numerical terminal or printer. Sometimes a VT55 terminal and its hard-copy unit is useful, especially in the polinomial fitting of the calibration curves. In general, graph terminal and

plotter are not necessary, but their including and the improvement of the RIPP are coming in future.

The RIPP consists of about 20 single programs written on FORTRAN IV—PLUS which execute about 35 different procedures. All programs process the image

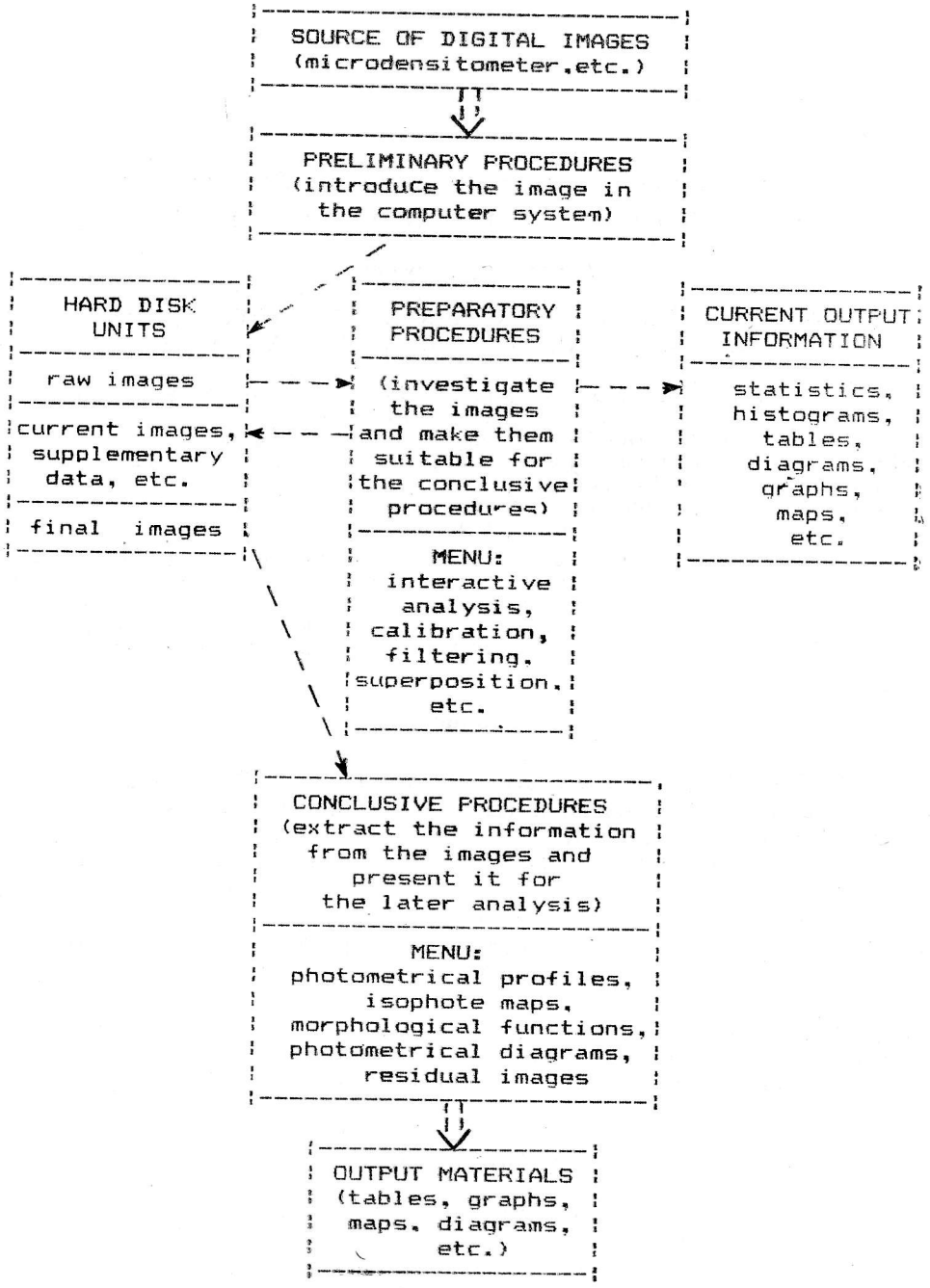


Scheme 1. A general view of the Rozhen Image Processing Package (RIPP).

row-by-row, in a sequential access mode. Sometimes, e. g. in the filtering procedures, a few sequential rows reside in the memory simultaneously. In the RIPP an arbitrary format is adopted and always the block size in the file corresponds to the width of the image in pixels.

The width of the image can be more than 1000 pixels and there is no practical

TABLE 1

**The data about the plates and the digital images used for the illustrations**

| Fig. No. | Object | | Telescope, system | | Observer | Pixel [mic] | Image | Zero level | Interval | System |
|---|---|---|---|---|---|---|---|---|---|---|
| 1 | Akn 319 | 3 | ZU21 | *B* | H. Markov | 25 | 128×128 | 0 | 0.1 | *D* |
| 2 | Digital simulated and noised image | | | | | | 29×40 | 50 | 50 | Units |
| 7 | M 87 | 1 | ZU21 | *B* | B. Bilkina | 100 | 100×128 | 0.36 | 0.06 | *D* |
| 8 | M 31 | 2 | 103aE | *R* | F. Borngen | 300 | 60×60 | 0.1 | 0.05 | *D* |
| 9 | GZ comet | 1 | ZU21 | pg | V. Ivanova | 100 | 37×101 | 0.65 | 0.075 | *D* |
| 10 | NGC 205 | 1 | ZU21 | *B* | T. Georgiev | 100 | 43×32 | 0.2 | 0.2 | *D* |
| 11 | M 31 | 2 | 103aD | *V* | F. Borngen | 300 | 150×520 | 0 | 25 | Units |
| 12 | M 31 | 1 | 103aOD | *BV* | T. Georgiev | 300 | 65×260 | 0.45 | 0.15 | *B—V* |
| 14 | H comet | 3 | ZU21 | pg | T. Bonev | | 30×30 | — | 0.008 | lg I |
| 15 | M 81 &Co. | 1 | ZU21 | *B* | B. Bilkina | 1000 | 65×70 | 0.02 | 0.02 | *D* |
| 18—20 | M 31 | 2 | Kodak | *UBV* | F. Borngen | 300 | 150×520 | — | — | *UBV* |

1: The Rozhen 50/70 cm Schmidt telescope; scale 120″/mm
2: The Tautenburg 134/200 cm Schmidt telescope; scale 51.7″/mm
3: The Rozhen 2 m RCC telescope; scale 12.9″/mm

limit for its length, but using only a printer as a mapping device, the preferable width is up to 524 pixels. The single processing time of a 500×500 pixels image is up to several minutes, except the filtering procedures some of which continue up to several hours.

Further on a brief information about the basic options and some methods of the RIPP are given. More detailed data about the presented examples are colected in Table 1.

## 3. Preparatory procedures

### 3.1. Interactive analysis

This is the most usable sequence of facilities because after the analysis of the image a user can optimize the future process. The three basic stages here are the histogram analysis, the map analysis, and the background analysis.

The histogram of the image (Fig. 1*a*) gives an important information about the common properties of the brightness distribution [14]. The position of the histogram maximum corresponds to the background level. The histogram and its statistics permit an easy selection of appropriate system of isophote levels and immediate building of a simple image map (Fig. 2). This first map of the image serves to select a set of clear areas for the detailed background analysis (Fig. 3). The inclination of the background can be corrected. The histogram of the background and its statistics (Fig. 1*b*) serve building of a more expedient map of the image. Thus, a user can fastly build also the conclusive map, that corresponds best to his task and to the individual properties of the image [15].

### 3.2. Calibration

Normally we use the known profiles of the galaxies and the corresponding densities, taken from the scanned image as a linear section (a program that takes a non-linear situated set of data is coming). Further on an interactive procedure with orthogonal polinomials in the method of the little squares fits the calibration function. So, in case of bright parts of the images we receive the calibration function directly, with no background estimation. Then the using of the logarithm of density as a calibration parameter is very comfortable (Fig. 4), because no more data are necessary and only 3rd—5th degree polinomial is enough [16—17]. The user controls the result by means of a VT55 terminal. The calibration function is

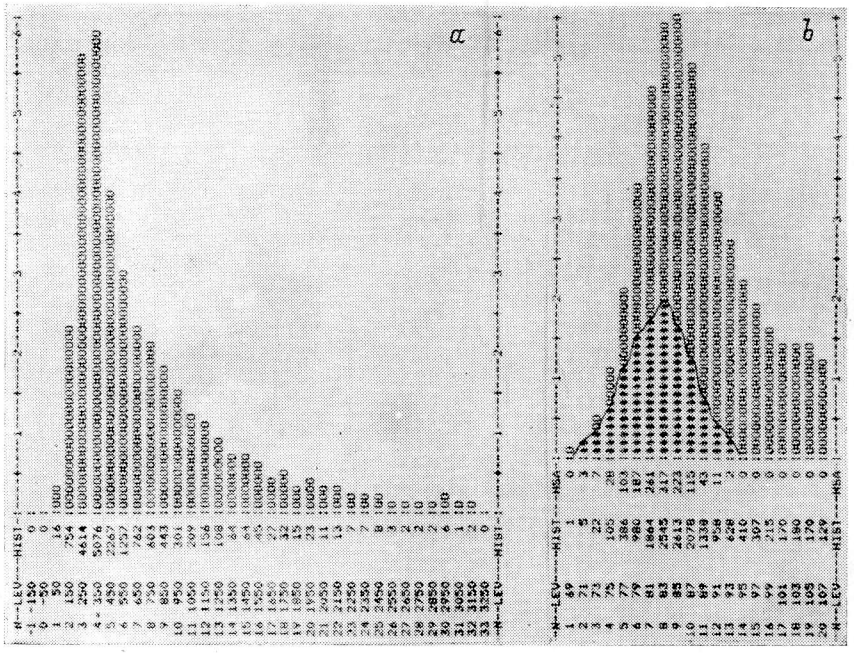


Fig. 1. Typical histograms of a galaxy image.

*a* — whole histogram; *b* — the region of the maximum with a subhistogram obtained from few clear background areas.

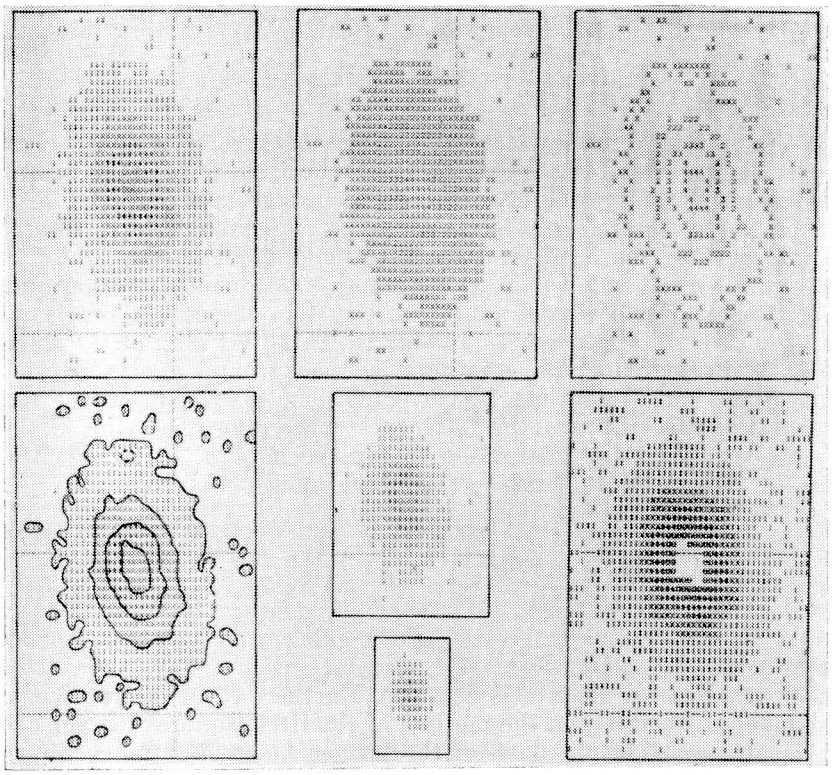

Fig. 2. Different appearences of the alpha-numerical maps built by the printer.

The smaller maps show the image under reductions which can go in the process of the mapping.

valid in a limited brightness interval and this is forseen in the calibration transformation of the image. The usual calibration procedure including linearization by means of the wedge is also program ensured.

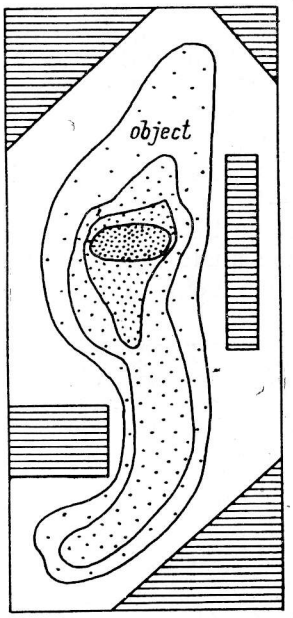


Fig. 3. Examples of the possible background areas around the object.

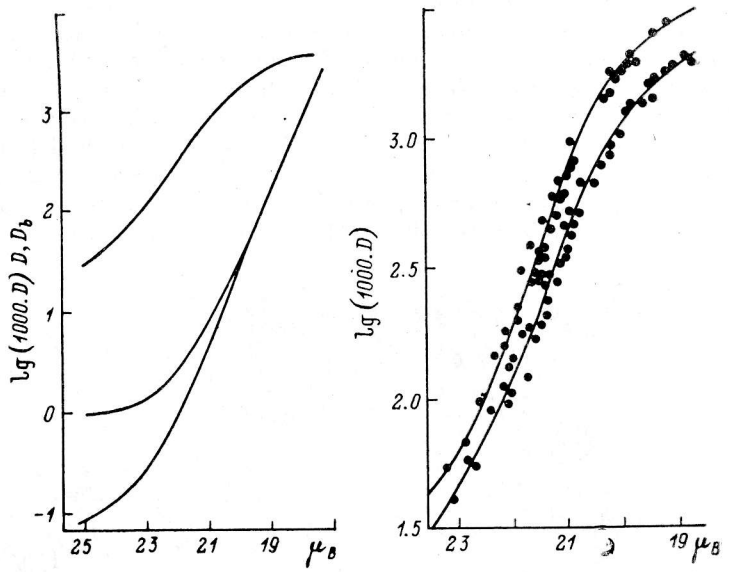


Fig. 4. Calibration curves.

*a* — appearances of the calibration curve when various parameters are used — densities $D$, baker densities $D_b$, and logarithm of densities lg $D$; *b* — two calibration curves with lg $D$, that are used for the compared images in Fig. 11.

### 3.3. Convolute filtering

The direct two-dimensional convolution of the image with a suitable smoothing function, so called nucleus, is a well known method. It can suppress effectively the gauss-like noise due to the emulsion granularity (see g. [3]). An unusual

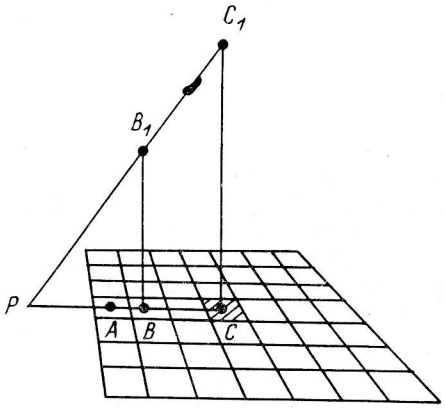


Fig. 5. The rule of the cone nuclei formation (see the text).

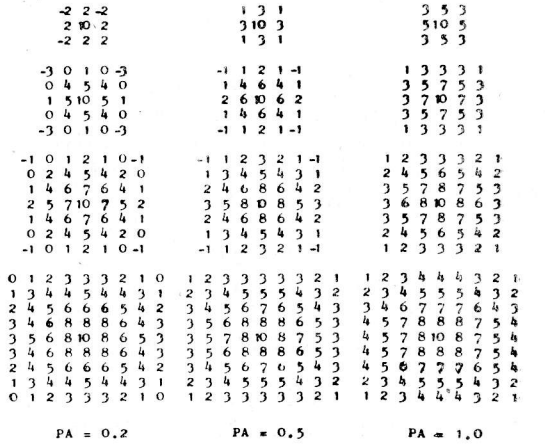


Fig. 6. Approximate appearance of three systems of cone nuclei shown before their normalyzing.

application of this method was given in [18] as a slide average smoothing only of the faint parts of the image. This method decreases the resolution, but increases the signal-to-noise ratio (S/N) and gives evidences of the extended faint periphery of

the image. In the RIPP such approach is enlarged and the convolute filtering is realized as a brightness depending method.

The input brightness threshold $V1 < V2$ divide the image into three brightness intervals: faint, middle and bright. The program prepares preliminary a system of nuclei with dimensions $3\times3$, $5\times5$, ..., $w\times w$, ... $W\times W$ elements. When the current processed pixel of the image has a value $V < V1$, only the nucleus with $w=W$ is used and a strong smooth effect is reached. If $V > V2$, the current pixel outputs to the processed image unchanged. When $V1 < V < V2$, at first the nucleus with $w=3$ is used and the value $V3$ is produced. If $V1 < V3 < V2$, the nucleus with $w=5$ is used and the value $V5$ is produced, etc. The process continues untill $w=W$ or $Vw < V1$ or $Vw > V2$ is reached [15—16]. Thus, a graceful transition between the smoothed and unprocessed parts of the image is ensured.

If only suppressing of the noise is necessary, the gaussian nucleus is the best. However, a nucleus which is not so different from the gaussian and which is close

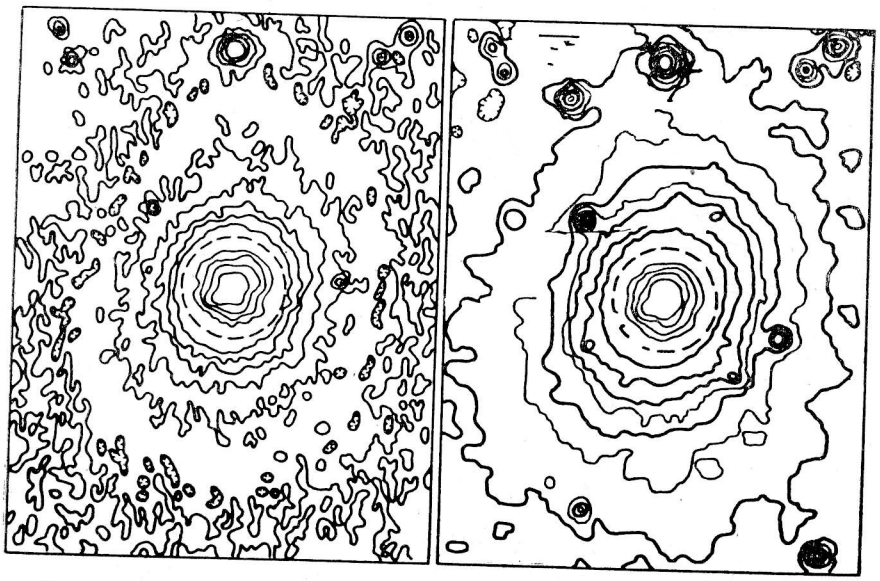

Fig. 7. Application of the convolute filtering method to the M87 galaxy image aiming to smooth its periphery.

The central part, given under 3.7 fold enlargement, is saved.

to the cone is suitable also [3]. If such a nucleus has appropriate negative peripheral elements, it causes certain restoration effect. This is useful in the bright part of the image, where the S/N is relatively high.

The form of the cone nuclei is easily managed as follows. In Fig. 5 the elements of the nucleus with $w=7$ are presented as squares. The value of the central element is given by $CC_1$ and the value of the arbitrary one is given by $BB_1$. The inclination of $C_1P$ to the plane shows the decrease of the nucleus elements depending upon the distance from the centre $C$. The equations $BB_1/CC_1=PB/PC$, $PB=PA+AC-BC$ and $PC=PA+AC$ lead to the expression $BB_1=CC_1[1-BC/(PA+AC)]$. Here $CC_1$-const, $BC$ is the distance from the centre, $AC$-mod$(w/2)$ and only $PA$ is the free parameter, that can change the cone angle. Some examples of such nuclei (before the normalyzing) are given in Fig. 6. The values $PA=0.2$—$0.3$ can cause restoration, $PA=0.5$ causes smoothing without notable loosing of the resolution, and $PA > 1$ causes smoothing like to the slide average.

The suitable use of the input parameters, $W$, $V1$, $V2$ and $PA$ permits various possibilities of the convolute filtering method. The particular cases of the convolution of the image with a single fixed nucleus, as well as the peripheral smoothing only are usable. Occasionally, it is possible to smooth simultaneously the periphery of the image and to reach certain restoration in its brightest part, but the last mentioned effect must be especially verified in every case.

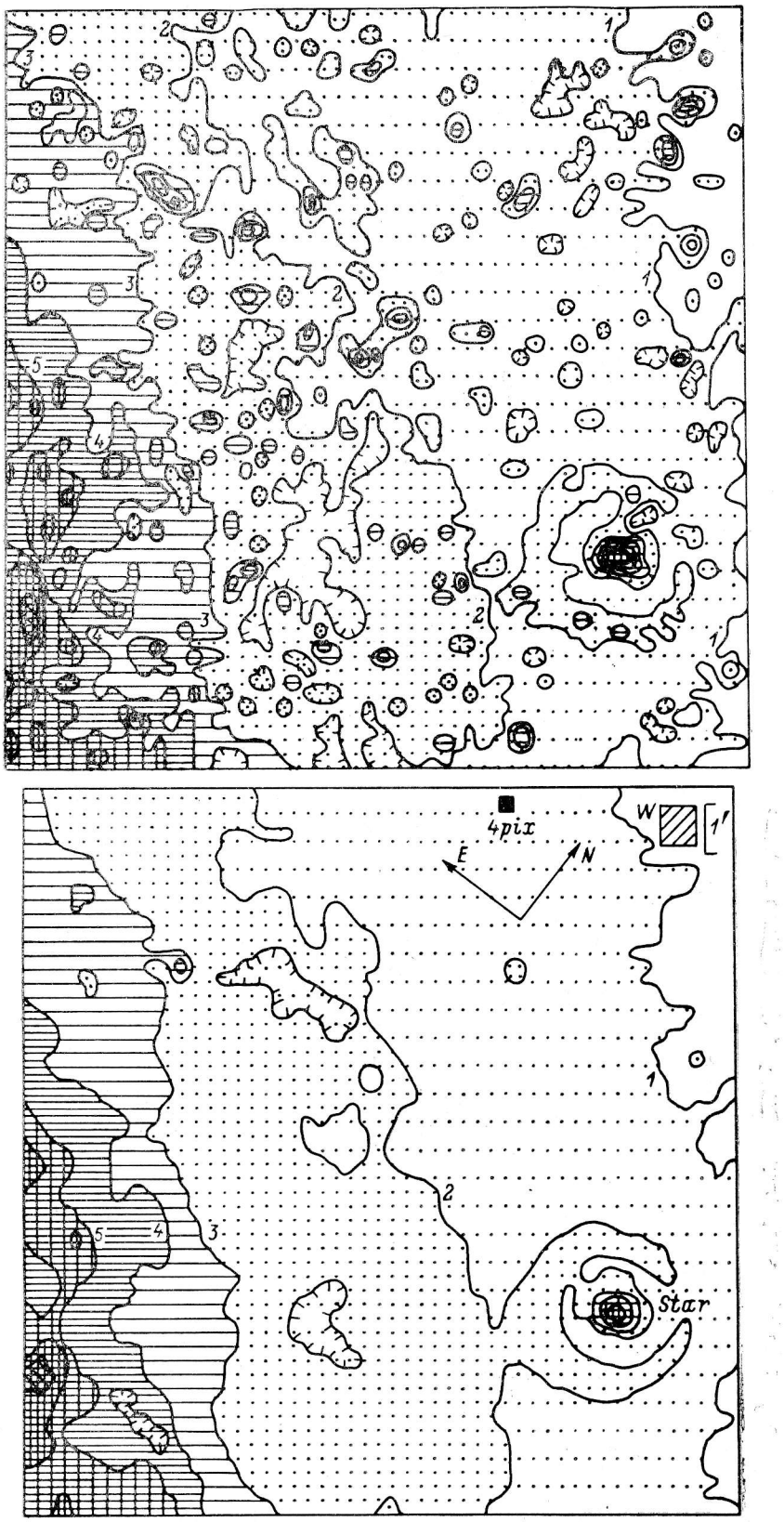


Fig. 8. Application of the median filtering method to the part of the M 31 galaxy image aiming to remove the stellar images and the emulsion gaps.

The window with size $w=3$ is used.

One application of the convolute filtering method to the M 87 galaxy is shown in Fig. 7 [15—16]. The input parameters have values $W=7$, $V1=0.4$, $V2=0.5$ and $PA=0.5$. The background level has a value $0.33+0.03$. so the lowest isophote level corresponds to $1\sigma$ above the background. The thin isophotes in the smoothed picture are the intermediates. After the peripheral smoothing, the shape of the image is visible clearly.

### 3.4. Median filtering

The median filtering method was proposed for the one-dimensional case in 1971 by Tukey [19]. This nonlinear procedure is useful in the two-dimensional case

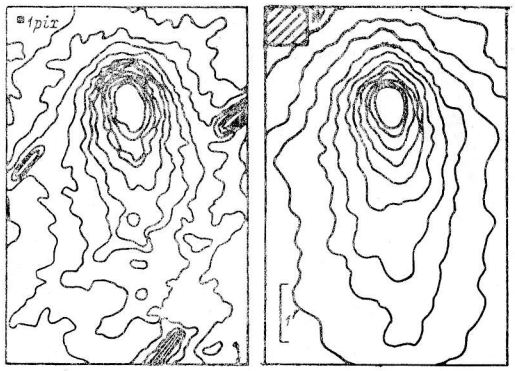


Fig. 9. Application of the median filtering method to the Gakobini-Zinner comet aiming to remove the stellar trecks.

Here $w=7$ is used.

perfectly, because it can remove various kinds of impulse noise [3, 20]. In the astronomical photographs such noises are caused by the foreground stellar images and the emulsion gaps.

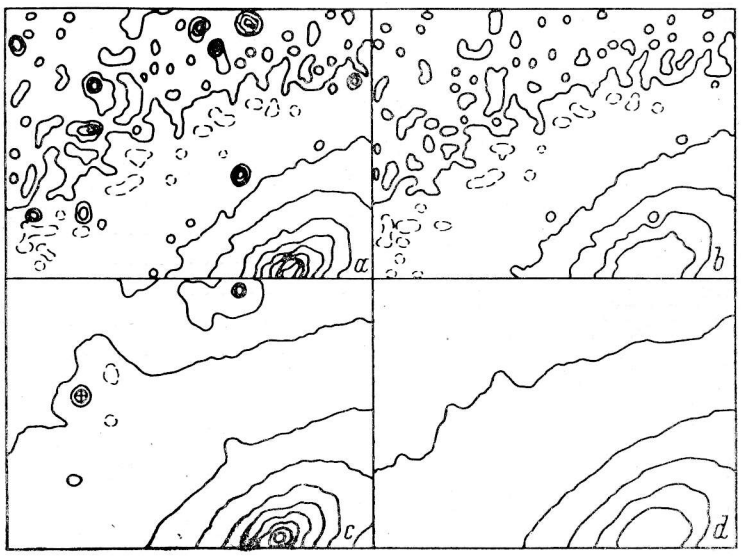


Fig. 10. Application of the median and covolute filtering to the NGG 205 galaxy image.

*a* — raw image; *b* — after median filtering only; *c* — after convolute filtering only; *d* — after cosequential application of the median and convolute filtering.

The action of the median filtering is similar to the slide average, where the average value is changed by the median value. The median is a robust estimation of the mean value because its dependence upon the noise impulses is neglected.

So, the image can be smoothed without residual local deformations due to the impulses. If the noise is gauss-like, the median value is practically equal to the average value and the median filtering is usable also.

It is very important for the practice that the median filtering can be enough fast. In the RIPP an algorithm similar to that described by Friden [20] is applied.

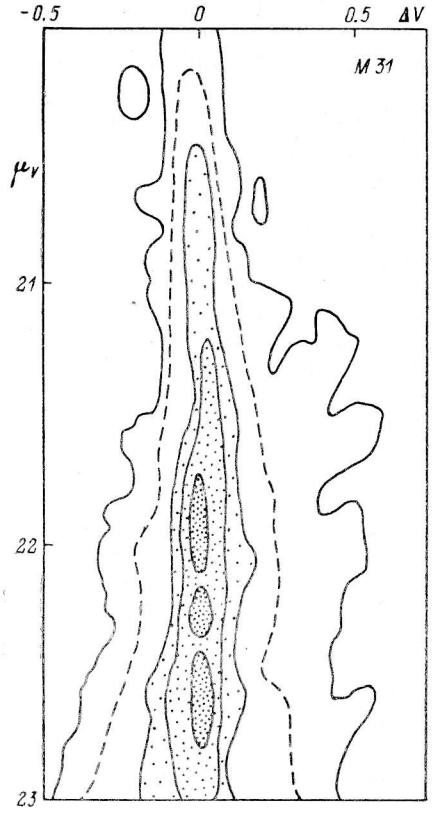


Fig. 11. The distribution of the differences between two averaged images depending upon the brightness.

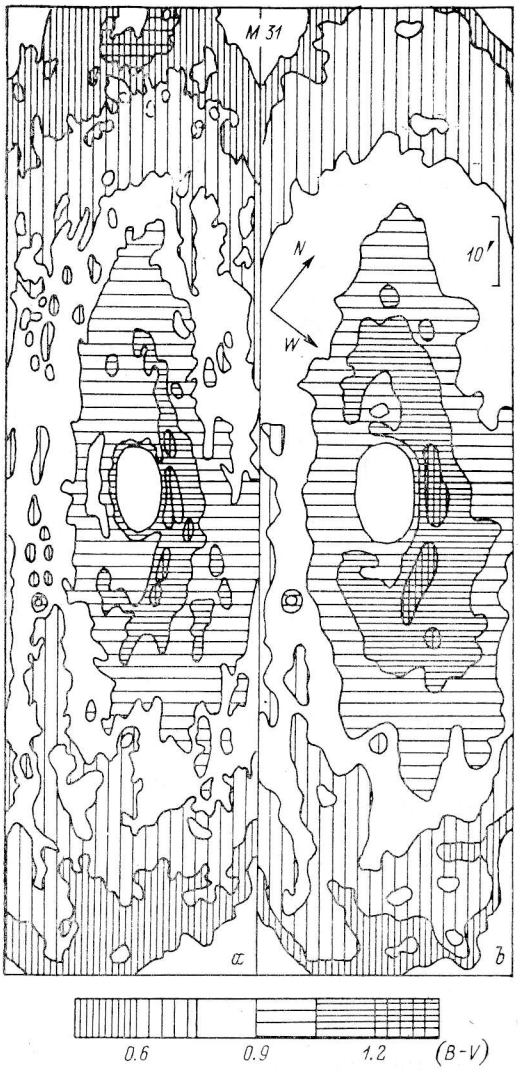


Fig. 12. The first isocolor map of the M 31 galaxy image [11, 16].

*a* — raw image; *b* — after smoothing [by convolution with $w=7$.

So, e. g. we can use the window size $W=65$ and the process of a $232\times300$ pixels image continue about 16 min. Now only the square windows are usable, but the inserting of circle-like and ring-like windows is coming.

Usual applications of the median filtering method, aiming to remove the stellar images and to suppress the noise, are given in Figs. 8 and 9. Both median and convolute filtering can be combined as it is shown in Fig. 10. The rough scanned image (*a*) contains unresolved stellar images and noise. The median filtering only (*b*) removes the stellar images (as well as the nucleus of the galaxy), but the noise rests. Here a special realization of the median filtering acts only if the difference between the current pixel value and the median value is larger than the chosen limit. The convolute filtering only (*c*) suppresses all kinds of the noise, but distri-

butes the «energy» of the stellar images over their surroundings. So, the bright stellar images deformate notably the isophote picture of the smoothed image. The consequential applying of the median and convolute filtering ($d$) removes the stellar images, suppresses the noise, and shows the clear shape of the image [12, 13, 16].

### 3.5. Superposition

This simple procedure can give the average from two images, aiming to suppress the noise. Then it is important to know the statistics of the differences between the corresponding pixels of the images $dV(i, k)=V1(i, k)-V2(i, k)$ depending on their average value $V(i, k)$. This information goes out as an alpha-numerical map. Each cell of the map shows the number of the pairs $[dV(i, k), V(i, k)]$ occured in the cell. In the example given in Fig. 11 the cell dimension is $0.05\times$ $\times 0.1$ m/□″ and the isolines correspond to the 0, 50, 100, 200, and 500 units per cell. It is clearly seen how the incorrespondence between the images grows up when the brightness grows down. The mean difference between the used $V$-images of the M 31 galaxy in the range 19—23 m/□″ is $0.017\pm 0.122$ m/□″.

In another case the superposition permits to receive the difference between two images, aiming to find any discrepancies, or to investigate the color distribution. The corresponding example, given in Fig. 12, shows the first color maps of the M31 galaxy [11, 21]. Note, the big red circle-like region in the near (right) part of the galaxy corresponds to the large gas and dust clouds between the spiral arms.

The superposition facilities can give also linear combination from a suitable set of images. This permits to investigate the distribution of reddening of free indices over the image.

### 3.6. Other procedures

There is a set of useful transformations in the RIPP that changes the atributes or the appearance of the image, according to the user's wish. These are sampling, reduction, expanding, rotation, etc., as well as a set of amplitude and gradient transformations.

An important addition to the described facilities is the method of the residual image, that is the subject of a separate paper in this volume.

## 4. Conclusive procedures

### 4.1. Photometrical profiles

This procedure gives final information about the brightness distribution along the arbitrary direction of the processing image. Our realization permits to receive the profile with a desired step and suitable pseudodiaphragm. The same procedure can take data for the calibration from already scanned image.

Each value of the received profile is obtained by means of a cone type distribution of the weight coefficients over the pixels inside the current position of the pseudodiaphragm. A suitable choice of the manage parameters (as in the convolute filtering method) permits to use a step of the profile that is up to 2 fold smaller than the image pixel. The output materials are graphs and tables, output by the printer, or graphs, drawn by a VT55 hard-copy unit.

Two examples about the M31 galaxy are presented in Fig. 13. The mean value of the $Q$-index in the bulge of this galaxy corresponds to an old stellar population. The increasing of $Q$ toward the centre can be explained by metal abundance growing and/or ageing of the stellar population, but this dilemma is not solved wholly for the present. The distribution of the $(U-V)$ (as well as of the other colors) confirms that the M 32 galaxy is situated before the M 31 galaxy plane [16].

## 4.2. Isophote maps

The maps give more complete information about the brightness distribution than the profiles. They permit also to find and anlyze single details of the image. Now in the RIPP the output maps are of alpha-numerical type, including the large maps, built by mens of the printer. The handling of such maps causes some

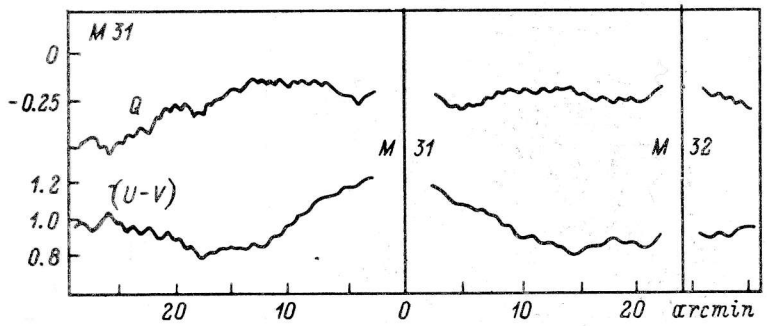


Fig. 13. The $Q$-and $(U-V)$-profiles of the M 31 galaxy image obtained from the corresponding images with step of 15″ and pseudodiaphragm 30″ [16].

practical difficulties, that will be overcome in the future by help of a plotter.

In Fig. 14 the isophote maps of the first photographs of the Halley's comet, taken in the Rozhen observatory, are shown. They are calibrated and smoothed by the convolute filtering method. It is interesting that all images have two nuclei and this fact is not explained till now [22].

An isodense map of the very faint brightness levels around the M 81 galaxy is shown in Fig. 15. This is the first evidence that the four bright galaxiea of the M 81 group are situated in a formation that is more bright than the night sky barely with $1+$ $+0.5$ %. The shape of this formation corresponds to the big gydrogen cloud in which the four galaxies are embedded [23].

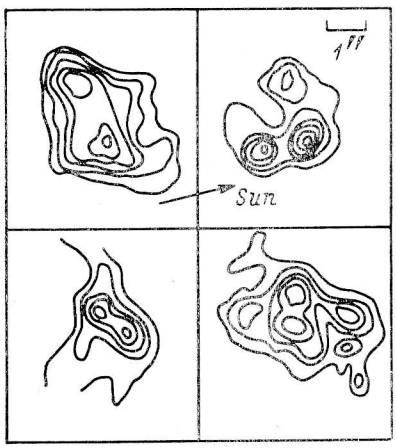


Fig. 14. The first four images of the Halley Comet obtained in the Rozhen observatory [22].

## 4.3. Morphological functions

Except profiles and maps of the image, often a summary of its morphological properties is needed. This is very important for the investigations of E—Sb galaxies, where a set of morphological parameters was used a long time ago.

The integral morphological parameters of an extended image (centriod, area, ellipcity and circularity parameters, magnitude and color, etc.) are defined above the given brightness threshold (see e. g. [8]). We introduce the differential morphological parameters, which give more detailed information than the integral parameters. They are the same as mentioned above, but defined for a specified brightness interval of the image [16, 24]. A few such intervals, limited by each pair of sequential isophote levels, are shown in Fig. 16.

The behaviour of the differential parameters (as dependences upon the brightness level or majorsemiaxis of the image) gives a generalyzed quantitative information about the morphology of the object. It is expedient to give the name of morphological functions to these dependences and to find a fast method for their obtaining.

In the RIPP the method of the image moments [25], is adopted to give the morphological functions [16, 24]. The corresponding program computes simultaneously the morphological parameters of 60—100 brightness intervals of the image,

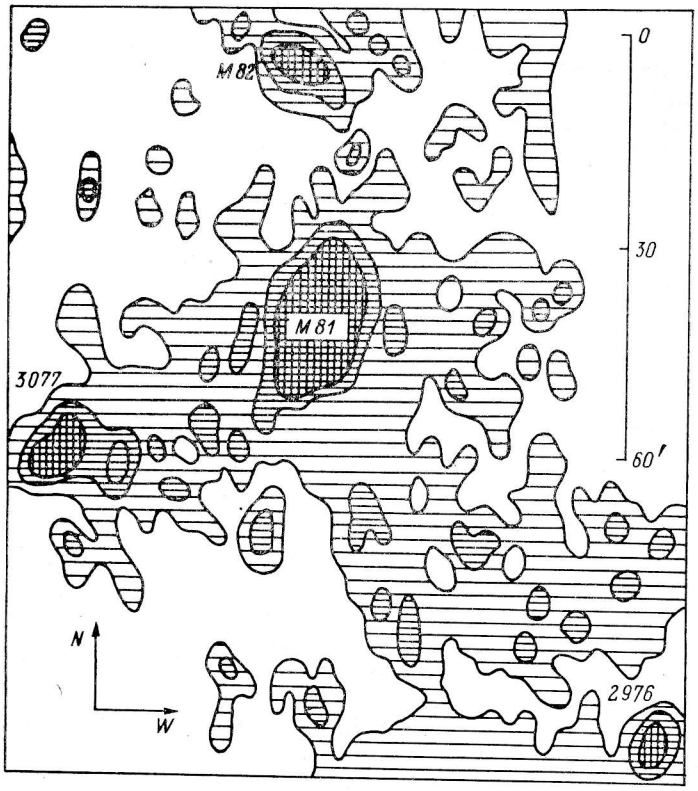


Fig. 15. The first evidence of the low brightness formation in the group of the M 87 galaxy [23].

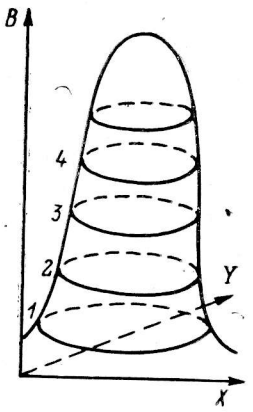


Fig. 16. Scheme of an image and its 4 brightness intervals.

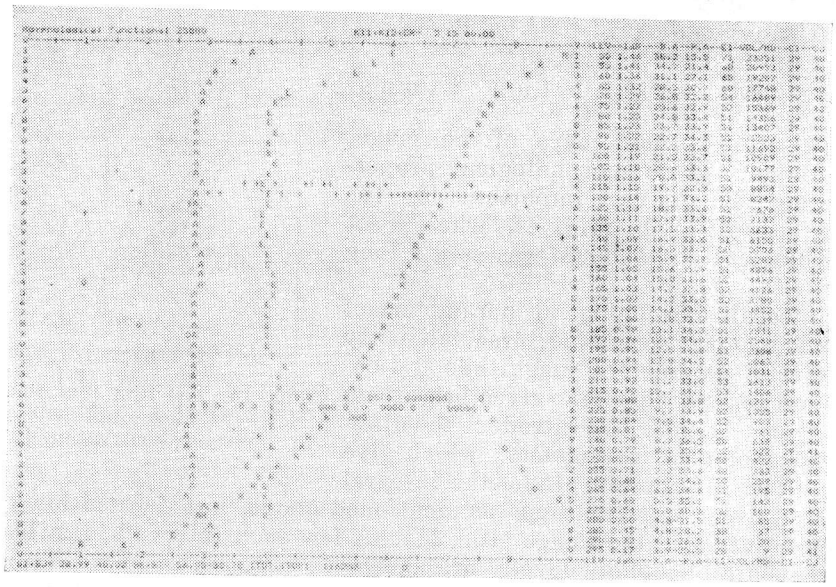

Fig. 17. The morphological functions of a digital simulated image presented by the printer as graphs and the corresponding table.

Each raw of the listing presents one brightness interval of the image.

each by size of 0.05—0.10 m/□″. The output materials are tables and graphs, which are printed as it is shown in Fig. 17.

The most usable morphological functions are the dependences of the brightness, colors, axial ratio $b/a$ and position angle upon the major semiaxis. The exam-

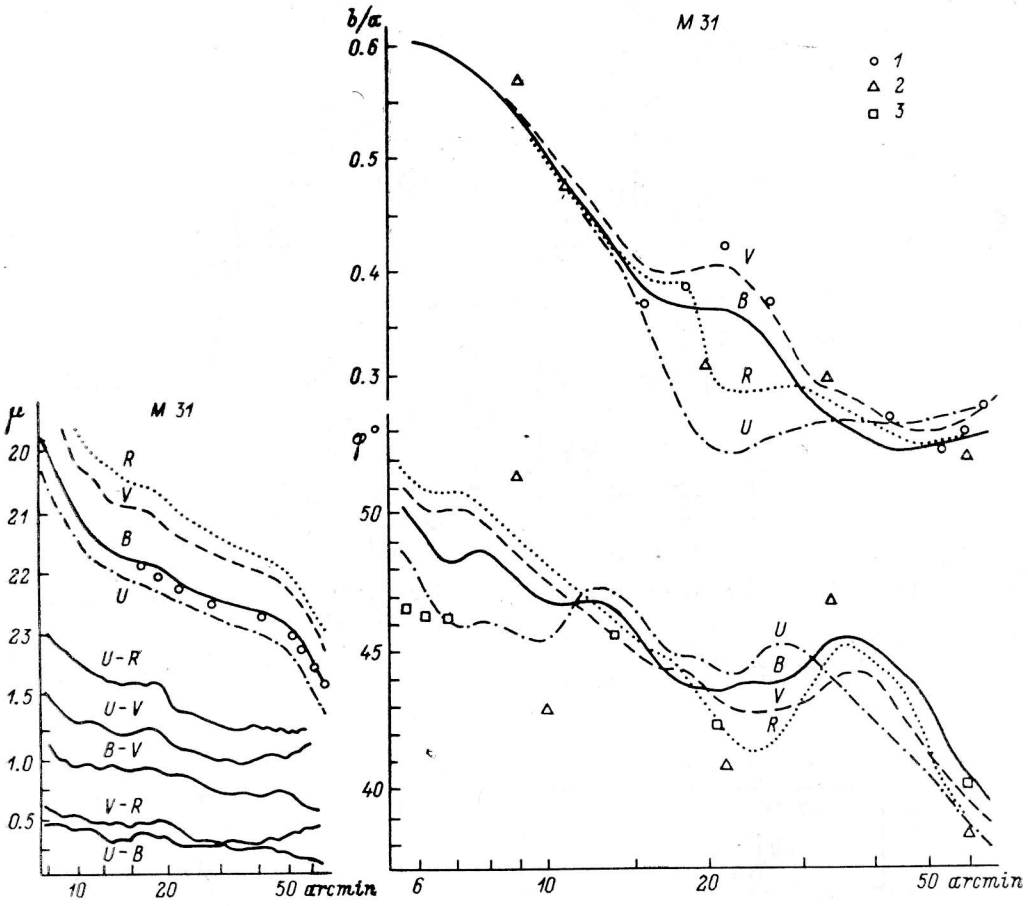


Fig. 18. High resolved morphological functions of the M 31 galaxy image in the *UBVR* system [24].

The single data from the other authors (only in *B*-light) are presented by circles (de Vaucouleurs), triangles (Richter and Högner) and squares (Hodge and Kennicutt).

ples in Fig. 18 show these functions of the M 31 galaxy image. This and the following examples are received by a process of 10 Tautenburg plates [16]. The analysis of the morphological functions in Fig. 18 considers that the M 31 palaxy has a two-armed trailing spiral structure and a bar in its central part [24].

### 4.4. Photometrical diagrams

The color-magnitude ($C—M$) and colo-colo ($C—C$) diagrams built by means of surface photometry data give valuable information about the stellar population of the investigate galaxy. The RIPP outputs such diagrams as alpha-numerical maps. Each cell of the map contains the number of the corresponding pair of values [e. g. ($B—V$, $V$)], occured in it. The best final appearance of the photometrical diagrams is the map of their isolines.

The examples shown in Fig. 19 are from the M 31 galaxy photometry [16, 26]. The first and the second diagrams are built independently by the plates from the Rozhen and Tautenburg Schmidt-telescopes. The results sre practically identical. All diagrams are given after an improving for the reddening effect and they show that the mean luminosity consistence of the M 31 galaxy has the spectral class GO.

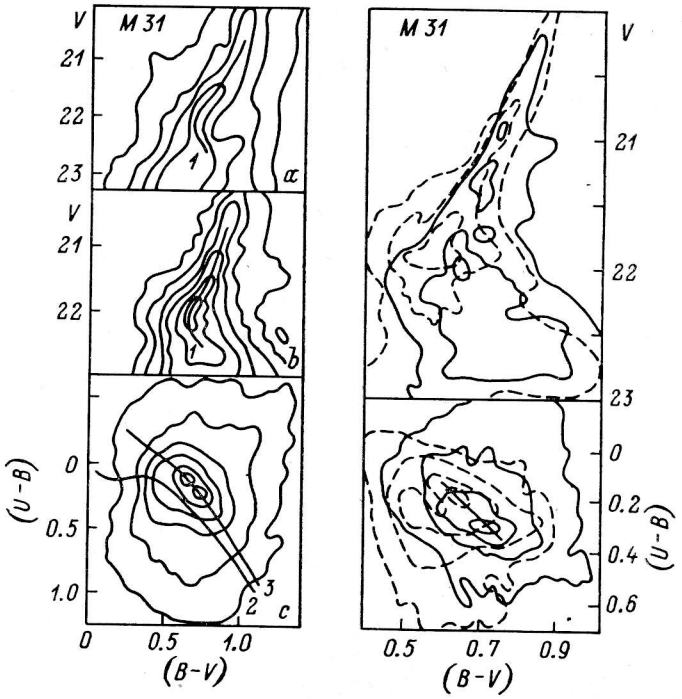


Fig. 19. Photometrical diagrams of the M 31 galaxy image obtained by the Rozhen (*a*) and the Tautenburg (*b*, *c*) Schmidt telescopes.

The lines show the main sequences of the globular cluster population (*1*), the normal colors of the 3rd class population (*2*) and the normal colors of the galaxies (*3*). The photometrical diagrams built separately for the distant contiguous line) and for the near (interrupted line) parts of the galaxy are shown in the right.

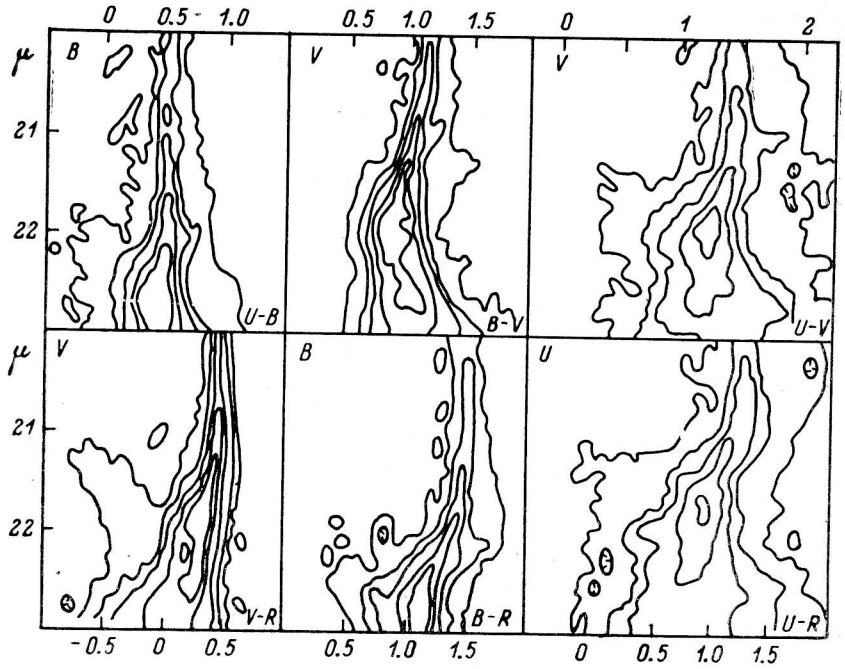


Fig. 20. Photometrical diagrams of the M 31 galaxy image in various appearance.

It is interesting that the shape of the $C-M$ diagram corresponds well to the line of the red giants of the globular clusters' population. Now this fact is not explained completely. The $C-C$ diagram has two maxima. The results of additional investigation of this phenomenon are shown in the right part of the Fig. 19. The diagrams are built separately for the far, south-eastern part of the image (contiguous line) and for the near, north-western part (dashed line). It is seen that the two maxima are caused by the two parts of the image, hence, due to the inclination of the M 31 plane [26]. A set of $C-M$ diagrams of M 31 is shown in Fig. 20.

## 5. Final remarks

The RIPP was created in close connection with the practice. It contains only a minimum number of useful procedures, but because of the independence of the programs, any improvements and enlargements are easy. The RIPP requires from the computer limited memory, and practically only a printer as an output device. Therefore, it is suitable for the microcomputer system also.

## 6. Acknowledgements

I am very grateful to my colleagues Drs. Y. Beilas, V. Golev, Z. Tsvetanov, G. Petrov and M. Tsvetkov for their valuable recommendations. I am very obliged also to Drs. J. Borissova, H. Nikov, G. Buyukliev and Eng. Yu. Staikov for the help in the practical work, as well as to Mrs. M. Kusheva for the help in the preparation of this paper.

### References

1. Andrews H. C., Enloe L. H. (Eds.) // Proceedings of the IEEE. 1972. **60**. No. 7. (in russian: 1973).
2. De Jager C., Nieuwenhui H. (Eds.) // Image processing techniques in Astronomy, D. Reidel Publ. Co. 1975.
3. Pratt W. K. // Digital Image Processing, John Willey and Sons, New York. 1978. (in russian: 1982).
4. Sedmac G. // Mem Soc Astron. Ital. 1986. **57**, P. 149.
5. Elliot J. (ed.) // Application of the Digital Image Processing to Astronomy, Proceedings of the SPIE. 1980. **264**.
6. Crane P., Kjar K. (Eds.) // Proceedings of the ESO Workshop on Two-dimensional Photometry, Noordwijkerhout, Holand, November. 1979. 1980.
7. Stobie R. S., McInnes B. (Eds.) // Workshop on the Astronomical Measuring Mashines (Occas. Rep. of the Roy. Observ. Edinburgh, 1983. No. 10.
8. Bijaoui A. // Eds. Sedmac et al. International Workshop on Image Processing in Astronomy, June 1979. Trieste, Italy. 1979. P. 173.
9. Bijaoui A. // Eds. Crane P., Kjar K. Proceedings of the ESO Workshop on Two-dimensional Photometry, Noordwijkerhout, Holand, November, 1979. 1980. P. 135.
10. Sedmac G. // Mem Soc. Astron. Ital. 1986. **57**, P. 149.
11. Georgiev T. B. // Lecture in the 12th National Week on Astronomy, Smolian, Bulgaria, September, 1985.
12. Georgiev T. B. // Preceedings of the 4th National Conference on Statistical Methods, October, 1986, Zlatni Piasatsi, Bulgaria. 1986a. **1**, P. 48.
13. Georgiev T. B. // Information Ensurence of the Space Experiments, Preceedings of the 8th Conference of the Section INTERCOSMOS-6, October, 1986, Stara Zagora, Bulgaria. 1986b. P. 87. (in russian).
14. Klinglesmith D. // Eds.: de Jager C. Nieuwenhuijzen H. Image Processing Techniques in Astronomy, D. Reidel Publ. Co. 1975. P. 271.
15. Georgiev T. B. // Proceedings of the 4th IAU Symposium on Astronomical photography, April, 1987, Jena, GDR. 1987a.
16. Georgiev T. B. // PhD Thesis, Bulgarian Academy of Sciences, Sofia, Bulgaria. 1987b.
17. Georgiev T. B. // Astrophys. Invest. Bulgar. Acad. Sci. 1989. **5**.
18. Jorsater S. // Preprint of the Stocholm Observatory. 1983.
19. Tukey J. W. // Exploratory Data Analysis, Addisson-Wesley Publ. Co. 1977. (in russian: 1981).

20. Friden B. // (Ed.) Computers in the Optical Research, Topics in Applied Phisics. 1980. **44**. Springer-Verlag (in russian: 1983).
21. Georgiev T. B. // Astron Zh. Letters. 1988b. **14**, P. 129.
22. Shkodrov V., Ivanova, V., Bonev T. // Proceedings of the 20th ESLAB Symposium on Exploration of Halley's Comet, Heidelberg, October, 1986, 1986. P. 195.
23. Getov R. G., Georgiev T. B. // Astron. Zh. Letters. 1988. **14**, P. 811.
24. Georgiev T. B. // Astron. Zh. Letters. 1988c. **14**, P. 882.
25. Stobie R. S. // Ed. Elliot J. Application of the Digital Image Processing to Astronomy, Proceedings of the SPIE. 1980. **264**. P. 209.
26. Georgiev T. B. // Astron. Zh. Letters. 1988d. **14**, 806.

Поступила в редакцию
4 июля 1988 г.